

High precision study of the Anderson transition

TOMI OHTSUKI¹KEITH SLEVIN²1) *Dept. Phys., Sophia University, Chiyoda-ku, Tokyo 102-8554, Japan*2) *Dept. Phys., Osaka University, Toyonaka, Osaka 560-0043, Japan*

(Dated: May 3, 2021)

INTRODUCTION

More than six decades have passed since Anderson's seminal paper on localisation was published[1]. During the subsequent decades, there have been numerous important discoveries including weak localisation, universal conductance fluctuations, and the scaling theory of localisation[2]. Localisation phenomena are observed not only in electron systems, but also in optical [3–9], acoustic [10–12], and cold atom systems [13–18].

Since the proposal of the scaling theory of localisation[19–23], determining the critical behavior of the localisation-delocalisation transition, which is usually referred to as the Anderson transition (AT), has continued to attract considerable attention. Depending on the symmetry of the Hamiltonian, systems are classified into orthogonal, unitary and symplectic symmetry classes, cf. the classification of random matrices[24, 25]. This classification was extended to include three classes with chiral symmetry[26, 27], and four classes with particle-hole symmetry[28]. These ten classes have also proven useful in the discussion of whether or not there is a topological phase and, if there is, what type of topological phase is realized, given the symmetry class and the dimensionality of the system.[29, 30]

In this activity report, we review the numerical approach for the study of the Anderson transition, and also another type of transition, the metal to semimetal transition. We emphasize the importance of the concept of universality class, and the scaling analysis of high precision numerical data.

The rest of this report is organized as follows. In the next section, we explain the method, followed by the results for our recent high precision studies of three dimensional (3D) Anderson transitions with and without time reversal symmetry. We then review the recent progress on the novel symmetry classes with chiral and particle-hole symmetries as well as the extension to non-Hermitian systems. We conclude this report by discussing the metal

to semimetal transition and the scaling behavior of the density of states.

METHODS

We start with the Anderson's model of localisation[1],

$$H = \sum_i E_i |i\rangle \langle i| - \sum_{\langle ij \rangle} |i\rangle V_{i,j} \langle j|. \quad (1)$$

where $|i\rangle$ is an orbital localised on site i of a 3D cubic lattice. The first sum is over all sites on the lattice and the second sum is over pairs of nearest neighbours. The unit of energy is the nearest neighbour transfer energy $V = |V_{i,j}|$, which we set to unity $V = 1$. The orbital energies E_i are assumed to be identically and independently distributed with a uniform distribution

$$p(E_i) = \begin{cases} 1/W, & |E_i| \leq W/2, \\ 0, & \text{otherwise.} \end{cases} \quad (2)$$

The parameter W determines the strength of disorder. The Hamiltonian commutes with the complex conjugation operator, i.e. a time reversal operator that squares to +1, and this model belongs to the orthogonal symmetry class [21, 22, 24, 25] (see Table I).

We can extend the Anderson model by including Peierls phases $V_{i,j} = \exp(i\theta_{i,j})$, which describe magnetic fields, in the nearest neighbour hoppings. Here $\theta_{i,j}$ with $i > j$ are randomly and uniformly distributed between $[0, 2\pi]$ and $\theta_{i,j} = -\theta_{j,i}$. We call this the U(1) model. In this case the Hamiltonian does not commute with a time reversal operator, and the model belongs to the unitary symmetry class.

Symmetry classification

We can further extend the model to include spin/orbital degree of freedom by modifying $V_{i,j}$ and E_i and can realize different symmetry classes.

Class	Symbol	TRS	PHS	CS
Unitary	A	No	No	No
Orthogonal	AI	1	No	No
Symplectic	AII	-1	No	No
Chiral Unitary	AIII	No	No	Yes
Chiral Orthogonal	BDI	1	1	Yes
Chiral Symplectic	CII	-1	-1	Yes
BdG	D	No	1	No
	C	No	-1	No
	DIII	-1	1	Yes
	CI	1	-1	Yes

TABLE I. Classification according to TRS, PHS and CS. For TRS (PHS), 1 means $C^T = C$ ($C'^T = C'$) whereas -1 means $C^T = -C$ ($C'^T = -C'$). BdG means Bogoliubov-de Gennes class.

Using the unitary operators C, C' and P , we can classify the Hamiltonian according to whether it satisfies the following symmetries[29],

$$H = CH^*C^{-1}, \quad (3)$$

for time reversal symmetry (TRS), and

$$H = -C'H^*C'^{-1}. \quad (4)$$

for particle-hole symmetry (PHS). Systems with TRS and PHS are further classified according to whether C or C' is symmetric or antisymmetric.

We also have chiral symmetry

$$H = -PHP^{-1}, P^2 = 1. \quad (5)$$

Note that chiral symmetry is automatic when we have both TRS and PHS.

The classification[29] is summarized in Table I.

The transfer matrix method

One of the ways to study the Anderson transition with high precision is to calculate the quasi-one dimensional localisation length and perform a finite size scaling analysis [31–35].

We consider a system with a square cross section $L \times L$, which we divide into layers labelled by their x coordinate. Then the Schrödinger equation for a state vector $|\Psi\rangle$ and energy E

$$H|\Psi\rangle = E|\Psi\rangle, \quad (6)$$

is expressed in the following form

$$\begin{pmatrix} \psi_{x+1} \\ V_{x+1,x}\psi_x \end{pmatrix} = M_x \begin{pmatrix} \psi_x \\ V_{x,x-1}\psi_{x-1} \end{pmatrix}, \quad (7)$$

where ψ_x is the wavefunction on the slice at position x ,

$$(\psi_x)_{y,z} = \langle x, y, z | \Psi \rangle. \quad (8)$$

M_x is the transfer matrix defined by,

$$M_x = \begin{pmatrix} V_{x,x+1}^{-1}(E - H_x) & -V_{x,x+1}^{-1} \\ V_{x+1,x} & 0_N \end{pmatrix}. \quad (9)$$

For the Anderson model where we set $V_{i,j} = -1$, we have

$$\begin{pmatrix} \psi_{x+1} \\ -\psi_x \end{pmatrix} = \begin{pmatrix} H_x - E & 1_N \\ -1_N & 0_N \end{pmatrix} \begin{pmatrix} \psi_x \\ -\psi_{x-1} \end{pmatrix}. \quad (10)$$

H_x is the following sub-matrix of the Hamiltonian

$$(H_x)_{y,z,y',z'} = \langle x, y, z | H | x, y', z' \rangle. \quad (11)$$

0_N and 1_N are the $N \times N$ ($N = L^2$) zero and unit matrices, respectively. The boundary conditions in the transverse directions influence some of the critical behavior[36]. In this report, we impose periodic boundary conditions in the transverse directions. We set the energy at the band centre, i.e. $E = 0$.

We note that the transfer matrix must satisfy the following relation

$$M_x^T \Sigma M_x = \Sigma, \quad (12)$$

where

$$\Sigma = \begin{pmatrix} 0_N & -i1_N \\ i1_N & 0_N \end{pmatrix}. \quad (13)$$

The wave-function amplitudes on the first two layers are related to the wave-function amplitudes on the last two layers as follows

$$\begin{pmatrix} \psi_{L_x+1} \\ -\psi_{L_x} \end{pmatrix} = M_{L_x} \cdots M_1 \begin{pmatrix} \psi_1 \\ -\psi_0 \end{pmatrix}, \quad (14)$$

which involves the product of L_x independently and identically distributed random matrices $M = M_{L_x} \cdots M_1$.

The following limiting matrix exists[37],

$$\Omega = \lim_{L_x \rightarrow \infty} \frac{\ln M^T M}{2L_x}. \quad (15)$$

The limit depends on the particular sequence of random matrices, but the eigenvalues $\{\gamma_i\}$ of Ω are the same for all sequences (“all” means with probability one). These values are called Lyapunov exponents. From Eq. (12) these eigenvalues occur in

pairs of opposite sign. It is usual to number them as follows

$$\gamma_1 > \cdots > \gamma_N > \gamma_{N+1} = -\gamma_N > \cdots > \gamma_{2N} = -\gamma_1. \quad (16)$$

This \pm symmetry can be derived from Eq. (12).

To estimate the Lyapunov exponents we start with a $2N \times 2N$ orthogonal matrix, truncate the matrix product at a very large but finite L_x , and perform a QR decomposition of the result

$$QR = MQ_0. \quad (17)$$

Here, Q_0 and Q are a $2N \times 2N$ orthogonal matrix and R is a $2N \times 2N$ upper triangular matrix with positive diagonal elements. We then define

$$\tilde{\gamma}_i = \frac{1}{L_x} \ln R_{i,i}. \quad (18)$$

In the limit of infinite length

$$\gamma_i = \lim_{L_x \rightarrow \infty} \tilde{\gamma}_i. \quad (19)$$

For sufficiently large L_x , the $\{\tilde{\gamma}_i\}$ may be used to estimate the Lyapunov exponents.

This method requires the simulation of a single very long sample. While this method has been employed very successfully in numerous simulations over the preceding decades, the calculations are inherently serial and do not allow us to take advantage of massively parallel computers.

Parallel transfer matrix method

An alternative way is to simulate an ensemble of much shorter samples and consider an ensemble average. While for simplicity we consider cubes with $L_x = L$, the method is also applicable when $L_x \neq L$.

We note here that the matrix Q_0 should be a $2N \times 2N$ random matrix with orthogonal columns sampled from a probability distribution that is invariant under convolution with the transfer matrix distribution, i.e., with a distribution that is invariant under the operation[38]

$$Q'R = M_x Q. \quad (20)$$

For such a distribution, it immediately follows that [39]

$$\gamma_N = \langle \tilde{\gamma}_N \rangle, \quad (21)$$

where $\langle \cdots \rangle$ is the sample average. To generate such matrices, we have found that the following procedure works well. We start with Q_0 given by the $2N$ -dimensional unit matrix,

$$Q_0 = 1_{2N} \quad (22)$$

and calculate

$$Q'R = M_q \cdots M_1 Q_0. \quad (23)$$

The matrix R is then discarded and we set $Q_0 = Q'$. This procedure is then repeated a sufficient number of times.

For a given L , we have found that, when a sufficient number of randomizing multiplications are performed, the distribution of $\tilde{\gamma}_N$ becomes independent of the number of such multiplications[39]. We assess this by applying the Kolmogorov-Smirnov test to the data for $\tilde{\gamma}_N$ with different numbers of randomizing multiplications. For sufficiently large number of randomizing multiplications we find that the Kolmogorov-Smirnov test is unable to distinguish the distribution of $\tilde{\gamma}_N$ obtained[39].

Fitting

Once we calculate γ_N , which is a function of the cross section size L and the strength of disorder W , we define

$$\Gamma(W, L) = L\gamma, \quad (24)$$

and assume the scaling form,

$$\Gamma(W, L) = F(\phi_1, \phi_2, \phi_3, \cdots). \quad (25)$$

Each scaling variable ϕ_i on the right hand side has a power law dependence on L

$$\begin{aligned} \phi_1 &\equiv u_1(w)L^{1/\nu}, \\ \phi_2 &\equiv u_2(w)L^{-y}, \\ \phi_3 &\equiv u_3(w)L^{-y'}, \\ &\cdots \end{aligned}$$

Here $1/\nu (> 0)$ is the scaling dimension of the relevant scaling variable and $-y$ is the scaling dimension of the least irrelevant scaling variable; $\cdots < -y' < -y (< 0)$.

In this report, we use the disorder strength W to tune the system through the transition. We denote the critical disorder where the transition occurs as

W_c . We define $w \equiv (W - W_c)/W_c$. The functions $u_j(w)$ ($j = 1, 2, \dots$) obey $u_1(w = 0) = 0$ and $u_j(w = 0) \neq 0$ ($j = 2, 3, \dots$). When w is sufficiently small, the u 's can be expanded in powers of w

$$u_i(w) \equiv \sum_{j=0}^{m_i} b_{i,j} w^j \quad (26)$$

with $i = 1, 2, \dots$, $b_{1,0} = 0$, and $b_{j,0} \neq 0$ ($j = 2, 3, \dots$)[35, 40]. When the ϕ 's are sufficiently small, the universal scaling function F can also be expanded[41]. We keep only the relevant scaling variable ϕ_1 and the least irrelevant scaling variable ϕ_2 , while assuming the other irrelevant scaling variables to be zero, $\phi_3 = \dots = 0$. This should be reasonable for w sufficiently small and L sufficiently large. We expand F in terms of ϕ_1 and ϕ_2 as

$$F = \sum_{j_1=0}^{n_1} \sum_{j_2=0}^{n_2} a_{j_1, j_2} \phi_1^{j_1} \phi_2^{j_2}. \quad (27)$$

To remove the ambiguity of fitting parameters, we set $a_{1,0} = a_{0,1} = 1$. The parameter $a_{0,0}$ is sometimes related to quantities of interest such as multifractal exponents[42], and we write it as Γ_c .

Whether the fit is plausible is determined by calculating the goodness of fit probability. When the fit is plausible, we check the stability of the fit against changes of the range of data being fitted and of the orders of the polynomial expansions. Fig. 1 shows an example of simulation data Γ and the results of the fitting.

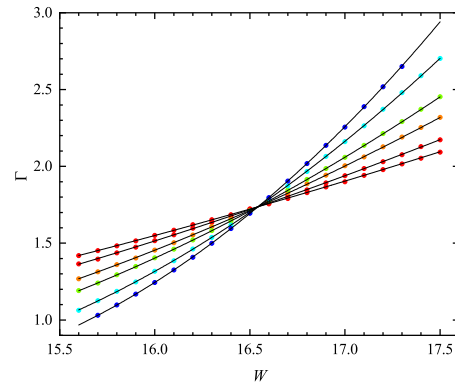
The confidence intervals of the fitting parameters are determined by Monte Carlo simulations. From the fitting function $F_i = F(W_i, L_i)$ for the i -th data ($1 \leq i \leq N_D$, N_D the number of data points), we produce an ensemble of synthetic data sets with $\tilde{\Gamma}_i = F_i + \sigma_i$ where σ_i is a random number, the variance is the same as that of i -th data and the mean zero. By fitting the synthetic data sets $\{\tilde{\Gamma}_i\}$'s we obtain the distribution of the critical parameters such as W_c and ν , and estimate their confidence intervals.

NUMERICAL STUDIES OF THE ANDERSON TRANSITION

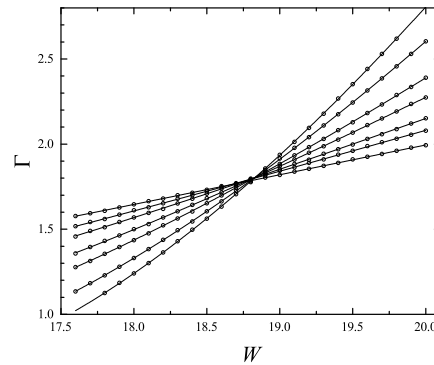
Wigner-Dyson classes

For the Wigner-Dyson (WD) classes, neither the particle-hole (PHS) or chiral (CS) is present. There

are 3 WD classes (see Table I). Using System B and simulating the Anderson and U(1) models, we have determined the critical exponents of the 3D orthogonal and unitary universality classes. The results are summarized in Fig. 1 and Table II.



(a) 3D class AI



(b) 3D class A

FIG. 1. Γ as a function of the disorder strength W for various cross section size L . (a) 3D class AI, where $L = 12, 18, 24, 32, 48$ and 64 . $L = 96$ is underway using new System B. (b) 3D class A, where $L = 4, 6, 8, 12, 16, 20$ and 24 . In the delocalised (localised) phase, Γ decreases (increases) with L . (a) is taken from [39] and (b) from [43].

The calculation time is proportional to the time for the QR decomposition and the number of transfer matrix multiplications. The dimension of transfer matrix is proportional to $L^{(d-1)}$, hence QR decomposition takes time proportional to $L^{3(d-1)}$, d being the space dimension. In addition, to obtain the same precision for larger L , we need to increase the length L_x proportional to L . The calculation time, therefore, is proportional to L^{3d-2} . This rapid increase of calculation time for higher dimen-

class	ν	Γ_c	W_c	N_D	N_P	p	$-y$
3D AI	1.572[1.566,1.577]	1.7372[1.7359,1.7384]	16.543[16.541,16.545]	117	7	0.5	–
3D A	1.443[1.437,1.449]	1.805[1.803,1.808]	1.805[1.803,1.808]	171	10	0.4	-3.1[-3.9,-2.4]

TABLE II. Results of the finite size scaling fits. Numbers are taken from Refs. [39, 43]. The systems sizes are $L = 24, 32, 48$ and 64 for 3D orthogonal class (Anderson model, class AI), whereas they are $L = 4, 6, 8, 12, 16, 20$ and 24 for 3D unitary class (U(1) model, class A). The precision is expressed by 95% confidence intervals, N_D is the number of data points, N_P the number of fitting parameters, and p the goodness of fit probability. For the 3D orthogonal case, irrelevant scaling variables are not necessary. This is because we use only $L \geq 24$ where corrections to scaling are smaller than the precision of the data [35].

sion, at first sight, gives the impression that higher dimensional simulation is almost impossible. However, the corrections to scaling are smaller in higher dimensions, and the critical behavior in dimensions higher than three has also been studied[43–45]. On the other hand, the critical behavior of the quantum Hall transition, which occurs in two dimensions, is still controversial due to the very slowly converging corrections to scaling[46].

Distribution of Kondo temperature

At the critical point, eigenstates exhibit multifractality. This is reflected in the fluctuations of the local density of states. As a result, when we consider magnetic impurities, the Kondo temperature T_K has a broad distribution. It has been predicted that the distribution of T_K has a power law tail at small T_K with a universal exponent whose value is related to the multifractal exponent η [47]. Using the kernel polynomial method [48], we calculated the local density of states at the Anderson transition, and determined the distribution of T_K . The massively parallel calculations on System B enabled us to reach the small T_K needed to check the analytic prediction [49]. Experimental verification may be possible by comparing with measurements of the temperature dependence of the magnetic susceptibility.

Beyond the Wigner-Dyson classes

Systems with CS/PHS symmetries have attracted much attention recently, because many of them are topological insulators or topological superconductors[29]. We note that these unconventional universality classes, i.e. classes other than Wigner-Dyson, are realized only at $E = 0$.

One way to realize a model with chiral symmetry

is to set all the orbital energies $E_i = 0$, and consider random hopping, $V_{i,j}$. Setting $E = 0$, we may then vary the strength of the randomness of the hopping and study the Anderson transition. This approach, however, has proven to be difficult to handle numerically because an unphysically large disorder in the hopping is needed to cause an Anderson transition[50].

Fixing the hopping and changing the diagonal disorder is easier for numerical calculations. This can be realized by considering, for example, the following Hamiltonian, which corresponds to 3D class CI (see Table I). It is a two-orbital cubic lattice model,

$$\begin{aligned}
\mathcal{H} &\equiv \sum_{\mathbf{i}, \mathbf{j}} \sum_{d, d'} |\mathbf{i}, d\rangle [\mathbb{H}]_{(\mathbf{i}, d | \mathbf{j}, d')} \langle \mathbf{j}, d'| \\
&= \sum_{\mathbf{i}} \left\{ (E_{\mathbf{i}} + \Delta) (|\mathbf{i}, a\rangle \langle \mathbf{i}, a| - |\mathbf{i}, b\rangle \langle \mathbf{i}, b|) \right. \\
&\quad + t_{\parallel} (|\mathbf{i}, a\rangle \langle \mathbf{i}, b| + |\mathbf{i}, b\rangle \langle \mathbf{i}, a|) \\
&\quad + t_{\perp} \sum_{\mu=x,y} \sum_{d=a,b} (|\mathbf{i} + \mathbf{e}_{\mu}, d\rangle + |\mathbf{i} - \mathbf{e}_{\mu}, d\rangle) \langle \mathbf{i}, d| \\
&\quad \left. + t'_{\parallel} (|\mathbf{i} + \mathbf{e}_z, a\rangle \langle \mathbf{i}, a| - |\mathbf{i} + \mathbf{e}_z, b\rangle \langle \mathbf{i}, b| + \text{h.c.}) \right\}. \tag{28}
\end{aligned}$$

Here $d, d' = a, b$ denotes the orbital index, $\mathbf{i} \equiv (i_x, i_y, i_z)$ with $\mathbf{e}_x = (1, 0, 0)$, $\mathbf{e}_y = (0, 1, 0)$ and $\mathbf{e}_z = (0, 0, 1)$ is the site index on the 3D cubic lattice. The orbital energies at two different lattice sites have no correlation; $\overline{E_{\mathbf{i}} E_{\mathbf{j}}} = \delta_{\mathbf{i}, \mathbf{j}} W^2 / 12$. The model has a particle-hole symmetry ($\mathbb{P} \mathbb{H} \mathbb{P}^{-1} = -\mathbb{H}$) as well as the time-reversal symmetry ($\mathbb{H}^* = \mathbb{H}$) with $[\mathbb{P}]_{(\mathbf{i}, d | \mathbf{j}, d')} \equiv (-1)^{i_x + i_y} \delta_{\mathbf{i}, \mathbf{j}} [\sigma_y]_{d, d'}$ with the 2 by 2 Pauli matrices, σ_x , σ_y and σ_z . Since $\mathbb{P}^T = -\mathbb{P}$, the Hamiltonian has a set of doubly degenerate real-valued eigenstates at zero energy, which results in the degeneracy of the Lyapunov exponents at $E = 0$; the degeneracy is protected by the particle-hole symmetry. For simplicity, we set $\Delta = t_{\parallel} = t'_{\parallel} = t_{\perp} = 1$. As in the previ-

ous subsection, the localisation length of the zero-energy eigenstates along the z -direction (λ_z) is calculated via the transfer matrix method. The periodic boundary condition is imposed along x and y directions. The density of states (DOS) of \mathbb{H} with finite disorder strength W is calculated in terms of kernel polynomial expansion (KPE) method [48]. Due to the particle-hole symmetry, the calculated DOS is symmetric about $E = 0$, while the DOS at $E = 0$ remains finite at the critical point [51]. The exponent of 3D class CI thus estimated is $\nu = 1.16 \pm 0.02$.

We can construct a similar Hamiltonian for the 3D class BDI, which is a model for disordered nodal-line Weyl semimetal [51].

SUMMARY AND CONCLUDING REMARKS

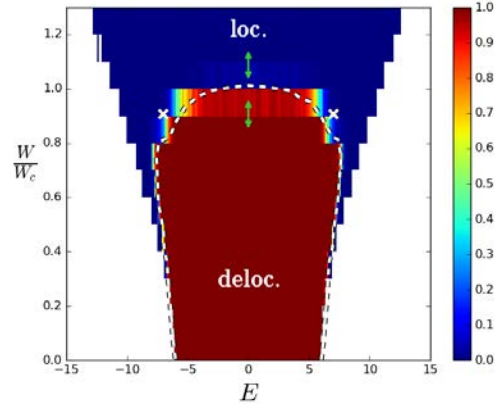
phase diagram

In this review, we focused on the Anderson transition at $E = 0$ (center of the band). Once we know the critical disorder $W_c \approx 16.54$ at $E = 0$ (see Table II), we can prepare thousands of delocalised ($W < W_c$) and localised ($W > W_c$) wave functions. Then we can let a convolutional neural network (CNN) learn the features of these wave functions [52, 53], and draw the phase diagram in $W - E$ parameter plane [54, 55].

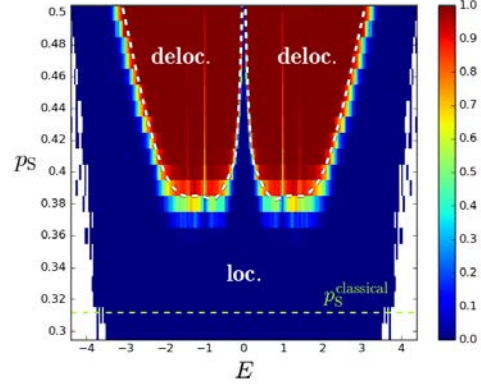
Fig. 2(a) is an example. We take the training regions indicated by the arrows in Fig. 2(a), and let the neural network calculate the probability that the states are delocalised in the rest of the parameter region. We can also draw the phase diagram for quantum percolation, where sites are present with probability p and absent with probability $1 - p$, and all the orbital energies are set to zero, $E_i = 0$. From the training in the Anderson model where the transfer matrix method is applicable, we can draw the phase diagram for the quantum percolation problem where the transfer matrix method is not applicable. Fig. 2(b) is the phase diagram for the quantum percolation problem drawn by the neural network trained using the Anderson model.

Beyond Hermitian classes

The symmetry classification according to TRS and PHS can be extended to non-Hermitian (NH)



(a) 3D Anderson model



(b) 3D quantum percolation

FIG. 2. Phase diagram of 3D Anderson transitions. (a) is for Anderson model. The green arrows in (a) indicate the regions where the CNN is trained, whereas the white dashed line and crosses indicate the phase boundary estimated by other methods [56, 57]. (b) is for site-type quantum percolation. The white dashed line is from the estimates by Ref. [58], whereas the green horizontal dashed line indicates the classical percolation threshold. Taken from Refs. [54, 55].

systems [59]. For example, for TRS for Hermitian systems we have $H = CH^*C^{-1} = CH^TC^{-1}$ [Eq. (3)], but for non-Hermitian systems there are two possibilities,

$$H = CH^*C^{-1}, H = CH^TC^{-1}. \quad (29)$$

The latter symmetry is straightforwardly realized for the Anderson model [Eq. (1)] by making the orbital energies E_j random complex numbers. We then have $H = H^T$ but $H \neq H^*$. The system is called NH class AI † . Making the E_j complex in the U(1) model realizes NH class A. The critical behaviors have been shown to be different from the Hermitian classes AI and A [60, 61] via the finite

size scaling analyses.

These two classes are only a part of the 38 symmetry classes[59] in non-Hermitian disordered systems. The critical behavior for these classes is an interesting topic left for the future.

Density of states scaling

So far, we have discussed the Anderson transition. There are other transitions in the same symmetry classes. For example, the semimetal to metal transition[62] occurs in 3D Dirac and Weyl systems, where the systems remains semimetal up to certain strength of disorder, then undergoes semimetal to metal transition. (Further increase of disorder leads to an Anderson transition.) Though the symmetry classes are AII (Dirac) and A (Weyl), the critical behaviors described by the scaling of the density of states[63, 64] is different from the Anderson transition, i.e., both the exponent ν and the dynamical exponent z differ from those of the Anderson transition in the same symmetry class and dimensionality.

Experiments

Interpreting the critical behavior found experimentally in doped semiconductors remains difficult because the role of the electron-electron interaction, which may be relevant in the renormalisation group sense, is not well understood. In experiments, the critical exponent s , which describes how the zero temperature conductivity vanishes as the critical point is approached from the metallic side, is measured. This exponent is related to the critical exponent ν by Wegner's relation $s = (d - 2)\nu$ [19]. As yet there is no agreement between theory and experiment and understanding the critical behaviour at the metal-insulator transition in doped semiconductors remains an open problem[65, 66].

The quantum kicked rotor with suitable quasi-periodic modulation exhibits an Anderson transition in the the same universality class as that in Anderson's model of localisation in 3D. This experimental realisation of the quantum kicked rotor has provided an alternative avenue for experimental investigation of the Anderson transition.[13–15]. The value $\nu = 1.63 \pm 005$ [15] found in these experiments agrees well with our numerical estimate.

Light waves [3, 4, 7–9] and acoustic waves [10–12] also localize and interaction effects play less of a role. For small loss, such systems are described by the 3D class AI. When the loss is not negligible, the system might show the critical behavior in 3D class AI[†]. Quantitative studies and detailed comparisons between theory and experiment are interesting topics left for the future.

Acknowledgement The work was partly supported by JSPS KAKENHI Grants 19H00658.

-
- [1] P. W. Anderson, Absence of diffusion in certain random lattices, *Phys. Rev.* **109**, 1492 (1958).
 - [2] E. Abrahams, ed., *50 Years of Anderson Localization* (World Scientific Publishing Company, 2010).
 - [3] S. John, Strong localization of photons in certain disordered dielectric superlattices, *Phys. Rev. Lett.* **58**, 2486 (1987).
 - [4] D. S. Wiersma, P. Bartolini, A. Lagendijk, and R. Righini, Localization of light in a disordered medium, *Nature* **390**, 671 (1997).
 - [5] M. Segev, Y. Silberberg, and D. N. Christodoulides, Anderson localization of light, *Nature Photonics* **7**, 197 (2013).
 - [6] A. Mafi, Transverse anderson localization of light: a tutorial, *Advances in Optics and Photonics* **7**, 459 (2015).
 - [7] T. Schwartz, G. Bartal, S. Fishman, and M. Segev, Transport and anderson localization in disordered two-dimensional photonic lattices, *Nature* **446**, 52 (2007).
 - [8] S. E. Skipetrov and I. M. Sokolov, Magnetic-field-driven localization of light in a cold-atom gas, *Phys. Rev. Lett.* **114**, 053902 (2015).
 - [9] S. E. Skipetrov, Localization transition for light scattering by cold atoms in an external magnetic field, *Phys. Rev. Lett.* **121**, 093601 (2018).
 - [10] T. R. Kirkpatrick, Localization of acoustic waves, *Phys. Rev. B* **31**, 5746 (1985).
 - [11] R. Weaver, Anderson localization of ultrasound, *Wave Motion* **12**, 129 (1990).
 - [12] H. Hu, A. Strybulevych, J. H. Page, S. E. Skipetrov, and B. A. van Tiggelen, Localization of ultrasound in a three-dimensional elastic network, *Nature Physics* **4**, 945 (2008).
 - [13] J. Chabé, G. Lemarié, B. Grémaud, D. Delande, P. Szriftgiser, and J. C. Garreau, Experimental observation of the anderson metal-insulator transition with atomic matter waves, *Phys. Rev. Lett.* **101**, 255702 (2008).
 - [14] G. Lemarié, J. Chabé, P. Szriftgiser, J. C. Garreau, B. Grémaud, and D. Delande, Observation of the anderson metal-insulator transition with atomic matter waves: Theory and experiment, *Phys. Rev. A* **80**, 043626 (2009).

- [15] M. Lopez, J.-F. Clément, P. Szrftgiser, J. C. Garreau, and D. Delande, Experimental test of universality of the anderson transition, *Phys. Rev. Lett.* **108**, 095701 (2012).
- [16] J. Billy, V. Josse, Z. Zuo, A. Bernard, B. Hambrecht, P. Lukan, D. Clément, L. Sanchez-Palencia, P. Bouyer, and A. Aspect, Direct observation of anderson localization of matter waves in a controlled disorder, *Nature* **453**, 891 (2008).
- [17] G. Modugno, Anderson localization in bose-einstein condensates, *Reports on Progress in Physics* **73**, 102401 (2010).
- [18] L. Sanchez-Palencia, D. Clément, P. Lukan, P. Bouyer, and A. Aspect, Disorder-induced trapping versus anderson localization in bose-einstein condensates expanding in disordered potentials, *New Journal of Physics* **10**, 10.1088/1367-2630/10/4/045019 (2008).
- [19] F. J. Wegner, Electrons in disordered systems. scaling near the mobility edge, *Zeitschrift für Physik B* **25**, 327 (1976).
- [20] E. Abrahams, P. W. Anderson, D. C. Licciardello, and T. V. Ramakrishnan, Scaling theory of localization: Absence of quantum diffusion in two dimensions, *Phys. Rev. Lett.* **42**, 673 (1979).
- [21] K. B. Effetov, A. I. Larkin, and D. E. Khmel'nitsukii, *Soviet Phys. JETP* **52**, 568 (1980).
- [22] S. Hikami, A. I. Larkin, and Y. Nagaoka, Spin-orbit interaction and magnetoresistance in the two dimensional random system, *Progress of Theoretical Physics* **63**, 707 (1980).
- [23] S. Hikami, Anderson localization in a nonlinear- σ -model representation, *Phys. Rev. B* **24**, 2671 (1981).
- [24] E. P. Wigner, On the statistical distribution of the widths and spacings of nuclear resonance levels, *Mathematical Proceedings of the Cambridge Philosophical Society* **47**, 790-798 (1951).
- [25] F. J. Dyson, Threefold way - algebraic structure of symmetry groups and ensembles in quantum mechanics, *Journal of Mathematical Physics* **3**, 1199 (1962).
- [26] R. Gade and F. Wegner, The $n = 0$ replica limit of $u(n)$ and $u(n)so(n)$ models, *Nuclear Physics B* **360**, 213 (1991).
- [27] R. Gade, Anderson localization for sublattice models, *Nuclear Physics B* **398**, 499 (1993).
- [28] A. Altland and M. R. Zirnbauer, Nonstandard symmetry classes in mesoscopic normal-superconducting hybrid structures, *Phys. Rev. B* **55**, 1142 (1997).
- [29] A. P. Schnyder, S. Ryu, A. Furusaki, and A. W. W. Ludwig, Classification of topological insulators and superconductors in three spatial dimensions, *Phys. Rev. B* **78**, 195125 (2008).
- [30] A. Kitaev, Periodic table for topological insulators and superconductors, *AIP Conference Proceedings* **1134**, 22 (2009).
- [31] A. MacKinnon and B. Kramer, One-parameter scaling of localization length and conductance in disordered systems, *Phys. Rev. Lett.* **47**, 1546 (1981).
- [32] A. MacKinnon and B. Kramer, The scaling theory of electrons in disordered solids: Additional numerical results, *Zeitschrift für Physik B Condensed Matter* **53**, 1 (1983).
- [33] J.-L. Pichard and G. Sarma, Finite size scaling approach to anderson localization, *J. Phys. C: Solid State Phys.* **C14**, L127 (1981).
- [34] B. Kramer and A. MacKinnon, Localization: theory and experiment, *Reports on Progress in Physics* **56**, 1469 (1993).
- [35] K. Slevin and T. Ohtsuki, Critical exponent for the anderson transition in the three-dimensional orthogonal universality class, *New Journal of Physics* **16**, 015012 (2014).
- [36] K. Slevin, T. Ohtsuki, and T. Kawarabayashi, Topology dependent quantities at the anderson transition, *Phys. Rev. Lett.* **84**, 3915 (2000).
- [37] V. I. Oseledec, A multiplicative ergodic theorem. characteristic lyapunov, exponents of dynamical systems, *Trans. Moscow Math. Soc.* **19**, 197 (1968).
- [38] K. Slevin, Y. Asada, and L. I. Deych, Fluctuations of the lyapunov exponent in two-dimensional disordered systems, *Phys. Rev. B* **70**, 054201 (2004).
- [39] K. Slevin and T. Ohtsuki, Critical exponent of the anderson transition using massively parallel supercomputing, *Journal of the Physical Society of Japan* **87**, 094703 (2018), <https://doi.org/10.7566/JPSJ.87.094703>.
- [40] K. Slevin and T. Ohtsuki, Corrections to scaling at the anderson transition, *Phys. Rev. Lett.* **82**, 382 (1999).
- [41] K. Binder, Critical properties from monte carlo coarse graining and renormalization, *Phys. Rev. Lett.* **47**, 693 (1981).
- [42] M. Janssen, Statistics and scaling in disordered mesoscopic electron systems, *Physics Reports* **295**, 1 (1998).
- [43] K. Slevin and T. Ohtsuki, Estimate of the critical exponent of the anderson transition in the three and four-dimensional unitary universality classes, *Journal of the Physical Society of Japan* **85**, 104712 (2016).
- [44] A. M. García-García and E. Cuevas, Dimensional dependence of the metal-insulator transition, *Phys. Rev. B* **75**, 174203 (2007).
- [45] Y. Ueoka and K. Slevin, Dimensional dependence of critical exponent of the anderson transition in the orthogonal universality class, *Journal of the Physical Society of Japan* **83**, 084711 (2014), <http://dx.doi.org/10.7566/JPSJ.83.084711>.
- [46] K. Slevin and T. Ohtsuki, Critical exponent for the quantum hall transition, *Phys. Rev. B* **80**, 041304 (2009).
- [47] S. Kettemann, E. R. Mucciolo, I. Varga, and K. Slevin, Kondo-anderson transitions, *Phys. Rev. B* **85**, 115112 (2012).

- [48] A. Weiße, G. Wellein, A. Alvermann, and H. Fehske, The kernel polynomial method, *Rev. Mod. Phys.* **78**, 275 (2006).
- [49] K. Slevin, S. Kettemann, and T. Ohtsuki, Multifractality and the distribution of the kondo temperature at the anderson transition, *The European Physical Journal B* **92**, 281 (2019).
- [50] A. M. García-García and E. Cuevas, Anderson transition in systems with chiral symmetry, *Phys. Rev. B* **74**, 113101 (2006).
- [51] X. Luo, B. Xu, T. Ohtsuki, and R. Shindou, Critical behavior of anderson transitions in three-dimensional orthogonal classes with particle-hole symmetries, *Phys. Rev. B* **101**, 020202 (2020).
- [52] T. Ohtsuki and T. Ohtsuki, Deep learning the quantum phase transitions in random two-dimensional electron systems, *Journal of the Physical Society of Japan* **85**, 123706 (2016), <http://dx.doi.org/10.7566/JPSJ.85.123706>.
- [53] T. Ohtsuki and T. Ohtsuki, Deep learning the quantum phase transitions in random electron systems: Applications to three dimensions, *Journal of the Physical Society of Japan* **86**, 044708 (2017), <http://dx.doi.org/10.7566/JPSJ.86.044708>.
- [54] T. Mano and T. Ohtsuki, Phase diagrams of three-dimensional anderson and quantum percolation models using deep three-dimensional convolutional neural network, *Journal of the Physical Society of Japan* **86**, 113704 (2017), <https://doi.org/10.7566/JPSJ.86.113704>.
- [55] T. Ohtsuki and T. Mano, Drawing phase diagrams of random quantum systems by deep learning the wave functions, *J. Phys. Soc. Jpn.* **89**, 022001 (2020).
- [56] S. L. A. de Queiroz, Reentrant behavior and universality in the anderson transition, *Phys. Rev. B* **63**, 214202 (2001).
- [57] G. Schubert, A. Weiße, G. Wellein, and H. Fehske, Hqs@hpc: Comparative numerical study of anderson localisation in disordered electron systems, in *High Performance Computing in Science and Engineering, Garching 2004*, edited by A. Bode and F. Durst (Springer Berlin Heidelberg, Berlin, Heidelberg, 2005) pp. 237–249.
- [58] L. Ujfalusi and I. Varga, Quantum percolation transition in three dimensions: Density of states, finite-size scaling, and multifractality, *Phys. Rev. B* **90**, 174203 (2014).
- [59] K. Kawabata, K. Shiozaki, M. Ueda, and M. Sato, Symmetry and topology in non-hermitian physics, *Phys. Rev. X* **9**, 041015 (2019).
- [60] X. Luo, T. Ohtsuki, and R. Shindou, Universality classes of the anderson transitions driven by non-hermitian disorder, *Phys. Rev. Lett.* **126**, 090402 (2021).
- [61] X. Luo, T. Ohtsuki, and R. Shindou, Transfer matrix study of the anderson transition in non-hermitian systems (2021), arXiv:2103.05239.
- [62] E. Fradkin, Critical behavior of disordered degenerate semiconductors. ii. spectrum and transport properties in mean-field theory, *Phys. Rev. B* **33**, 3263 (1986).
- [63] K. Kobayashi, T. Ohtsuki, K.-I. Imura, and I. F. Herbut, Density of states scaling at the semimetal to metal transition in three dimensional topological insulators, *Phys. Rev. Lett.* **112**, 016402 (2014).
- [64] S. Liu, T. Ohtsuki, and R. Shindou, Effect of disorder in a three-dimensional layered chern insulator, *Phys. Rev. Lett.* **116**, 066401 (2016).
- [65] Y. Harashima and K. Slevin, Critical exponent of metal-insulator transition in doped semiconductors: The relevance of the coulomb interaction, *Phys. Rev. B* **89**, 205108 (2014).
- [66] E. G. Carnio, N. D. M. Hine, and R. A. Römer, Resolution of the exponent puzzle for the anderson transition in doped semiconductors, *Phys. Rev. B* **99**, 081201 (2019).